

Artificial Life in an Exciton-Polariton Lattice

R. Banerjee and T.C.H. Liew*

*Division of Physics and Applied Physics, School of Physical and Mathematical Sciences,
Nanyang Technological University, Singapore 637371, Singapore*

E-mail: timothyliw@ntu.edu.sg

We show theoretically that a lattice of exciton-polaritons can behave as a life-like cellular automaton when simultaneously excited by a continuous wave coherent field and a time-periodic sequence of non-resonant pulses. This provides a mechanism of realizing a range of highly sought spatiotemporal structures *under the same conditions*, including: discrete, oscillating, and rotating solitons; breathers; soliton trains; guns; and chaotic behaviour. These structures can survive in the system indefinitely, despite the presence of dissipation and disorder, and allow universal computation.

Keywords

Exciton-Polaritons, Optical solitons, Pattern formation, Optical bistability.

Introduction

Exciton-polaritons are quasiparticles typically formed in microcavities where light hybridizes with excitons contained in quantum wells. As a result of this hybridization, (exciton)-polaritons have been used to study a variety of fundamental nonlinear effects, with a general motivation of reaching optoelectronic devices.¹ To give a few examples, a large body of work was focused on the creation and control of polariton solitons,²⁻⁸ which were conjectured to

play a role in devices^{9–11} with some soliton logic gates constructed.¹² In parallel, polaritons were found to form spatial patterns,^{13–18} where topologically stable structures were considered as a memory^{19,20} and pattern transitions could effectively compose switches.²¹ There has also been a growing interest in studying polaritons in periodic potentials,²² which have allowed the routing of polaritons,^{23,24} gap and lattice solitons,^{25–27} and the formation of spin-ordered patterns²⁸ for information processing.

While the aforementioned works are promising for polaritonic devices in principle, a complication in applying the aforementioned phenomena is that they have been found under different conditions in different parameter ranges. Here, we consider whether solitons, stable structures, and evolving patterns can co-exist *under the same conditions*, together with the analogues of a variety of other soliton-related structures studied separately in the literature, including: oscillating solitons and patterns;^{29–31} guns³² and soliton trains;^{6,9,10} soliton explosions;³³ and backward radiation emitting solitons.³⁴ We also aim for polariton solitons and related structures to exist indefinitely^{35, 19} beyond the finite polariton lifetime, and survive the presence of noise and disorder. To reach these aims, we attempt to associate a polariton lattice to a cellular automaton.

Cellular automata emerged as one of the first definitions of artificial life,³⁶ where they showed how remarkably complex behaviour associated to living organisms such as movement, growth, and replication can appear from apparently simple update rules applied on a lattice. The most commonly studied versions operate with square lattices, with each lattice site existing in one of two states typically referred to as “alive” or “dead”. An update rule is applied repeatedly, where the state of each lattice site is updated depending on its own state and the state of its neighbours. The update rule defines the complexity of the corresponding automaton, where four classes of increasing complexity exist.^{37–42} Sufficiently complex automata are known for forming spatial patterns, self-localized structures (i.e., solitons), gliders or spaceships (i.e., propagating solitons), breathers (i.e., oscillating solitons) and guns (that generate soliton trains). Cellular automata have applications in image pro-

cessing^{43–45} and those belonging to the most complex class (class 4) are typically universally (Turing) complete.⁴⁶ Life-like automata are defined as those where the update rule is based on the number of neighbouring alive states, independent of their relative position. Famous examples include Conway’s life and “Life without death”, which are universally complete class 4 automata.

There are reasons to expect that polaritons could operate as life-like automata. First, they can be confined in square lattices.^{26,47,48} Second, under continuous near-resonant coherent excitation, polaritons exhibit bistability,^{6,49} such that each site in a lattice would be in a high intensity (i.e., “alive”) or low intensity (i.e., “dead”) state for as long as the coherent excitation is maintained.⁵⁰ Furthermore the nonlinearity of polaritons suggests a potential for non-trivial behaviour, as the aforementioned works have demonstrated, however, it is a highly non-trivial question as to whether the nonlinearity can result in any complex automaton rules.

In addition to continuous near-resonant excitation, we consider the effect of non-resonant pulses applied to the system. Each pulse is found to initiate one update according to a life-like automaton rule, making use also of the spin-dependent interactions between polaritons⁵¹ and recently realized spin-orbit coupling in lattices.^{52,53} This provides a platform for merging many of the separately studied soliton-related polariton phenomena in microcavities and such combination shows most clearly their prospects for information processing: we find that *polariton solitons are universally complete*.

Scheme

Figure 1(a) shows a schematic illustration of a square lattice of polariton resonators (e.g., micropillars²²). Each resonator represents a “cell” supporting two polariton spin components

(σ_{\pm}), represented by the wavefunction $\psi_{n_{\pm}}$, which evolves according to:⁵⁵

$$i\frac{\partial\psi_{n_{\pm}}}{\partial t} = \left(-\Delta + |\psi_{n_{\pm}}|^2 + \alpha_2|\psi_{n_{\mp}}|^2 + iP_{\pm}(t) - \frac{i}{2}\right)\psi_{n_{\pm}} + J\sum_{\langle m \rangle}\psi_{m,\mp} + F_{\pm} \quad (1)$$

Δ represents an energy detuning between a driving laser field, with circularly polarized components F_{\pm} , and the resonant polariton energy. Spin-dependent interactions are accounted for, where the interaction strength between polaritons of parallel spin is scaled to unity (through appropriate choice of scale of $\psi_{n_{\pm}}$) and α_2 is the relative strength of interactions between polaritons with antiparallel spin. $P_{\pm}(t)$ represents a gain in the system,¹⁸ i.e., a non-resonant pulse with different spin components. The term $-i/2$ represents polariton dissipation (our time unit is the inverse dissipation rate).

We assume that each cell is coupled to its eight nearest neighbours (see Fig. 1(b)) through a spin-orbit coupling. In principle the spin-orbit coupling can be tuned through the design of the microcavity structure in the intermediate region between cells.^{52,53} It has also been shown that polaritons propagating in channels rotate their spins as they propagate,⁵⁶ allowing a design of a full inversion scheme of coupling which we assume between lattice sites here. We also assume an equivalent coupling for all neighbours (which requires that the effective potential for diagonal connections is engineered differently for horizontal/vertical connections). Although we consider here a tight-binding representation of polaritons, as is common for micropillar arrays,⁵² our results can also be reproduced with a continuous description (see sec.VII).

It is instructive to consider first the single cell behaviour ($J = 0$). In the stationary limit (with no pulse; $P_{\pm}(t)=0$), the stationary states of Eq. (1) excited by a σ_+ circularly polarized field ($F_- = 0$) show a well-known S-shaped dependence⁴⁹(see Fig. 1(c)) of the polariton intensity $|\psi_+|^2$ on the driving intensity $|F_+|^2$, given by $[(-\Delta + n_+ + \alpha_2 n_-)^2 + 1/4] n_+ = |F_+|^2$, where $n_{\pm} = |\psi_{\pm}|^2$. We fix F_+ throughout so as to remain in the bistable regime, where ψ_+ in each cell must adopt either a high intensity (“alive”) or low intensity (“dead”)

state in the stationary limit. The S-shaped curve depends on the detuning, Δ , which is effectively renormalized by the implantation of a population of σ_- polarized polaritons via the α_2 dependent term in Eq. (1) (see Fig. 1(c)).

In the limit of finite but small coupling between cells ($J \ll 1$), the coupling can be considered as a perturbation. It enters as an effective driving for σ_- polarized polaritons, where the field ψ_{n-} is driven by $J \sum_{\langle m \rangle} \psi_{m,+}$, according to Eq. (1). It is important that this field depends on the state of neighbouring cells, such that each cell is influenced based on how many of its neighbours are dead or alive (see Fig. 1(b)). In the perturbative limit, stationary states of σ_- polarized polaritons are given by $\psi_{m-} = F_{\text{eff}} / (\Delta - |\psi_{n-}|^2 - \alpha_2 |\psi_{n+}|^2 + \frac{i}{2})$, where $F_{\text{eff}} = J \sum_{\langle m \rangle} \psi_{m,+} + F_-$. We focus first on realizing the Life without death cellular automaton, which is characterized by the behaviour that a dead cell becomes alive if and only if it has three alive neighbours. All alive cells remain alive, such that any pattern developing in this automaton remains fixed. Figure 1(d) (lower points) shows the stationary states of ψ_{n-} for the case where a cell is initially dead and has different numbers of alive neighbours under the condition $P_{\pm}(t) = 0$ and $F_- = 0$. Choosing now a finite F_- will shift the stationary states. We choose $F_- = -J(3\psi_{\text{alive}} + 5\psi_{\text{dead}})$, where ψ_{alive} and ψ_{dead} represent the expected wavefunction of alive and dead neighbouring cells. This field, which will be fixed throughout, shifts the intensity of σ_- polarized polaritons to zero when a given cell has exactly three neighbours alive and otherwise leaves a finite intensity (Fig. 1(d)). Recalling Fig. 1(c), the S-shaped curve describing stationary states of σ_+ polarized polaritons should now be shifted if a cell has any number of neighbours alive other than three.

Having modified the stationary states of a cell in a neighbour-dependent way, we now consider the action of a non-resonant pulse, $P_{\pm}(t) = P_{\pm} e^{-\Gamma_R t}$. Physically, the pulse excites an exciton reservoir and we take the pulse as a decaying exponential to represent decay of the reservoir (with decay rate Γ_R). The two spin components of the pulse serve different purposes. The σ_- component amplifies the up until now weak population of σ_- polaritons, so that their neighbour dependent intensity has a more significant effect. At the same

time, the σ_+ component attempts to switch the state of σ_+ polarized polaritons to the alive state. Remarkably, we find that for well-chosen parameters (see sec. I) such switching is only possible when a cell has three alive neighbours, as shown in Fig. 2. For any number of neighbours different to three, the shift in the S-shaped curve has raised the threshold population needed to switch to the higher intensity state, such that the non-resonant pulse is insufficient.

While our scheme may appear complicated, involving different components of the coherent driving field F_+ and F_- as well as components of the non-resonant pulse P_+ and P_- , we note that these just correspond to specific polarizations of a continuous wave laser and a pulse. Both can be spatially uniform with no specific site to site modulation. Such pulse induced switching of a system driven by a continuous wave driving field is well within the limits of current technology.^{28,50,57-59} Each automaton update requires the application of just one pulse (see sec. V).

Conway's life and other cellular automata

We varied the parameters P_+ and P_- and found that different automata rules were possible. For example, the rule where a cell is born if it has three neighbours and survives if and only if it has less than seven neighbours alive was possible (see sec. I). This specific rule has not appeared in the literature but is also universally complete (see sec. I). More importantly, the presence of this rule shows that it is possible to realize the behaviour of overpopulation, where a cell dies if too many of its neighbours are alive. This allows more complex automata.

Conway's life requires that a cell is born if it has three neighbours and survives if and only if it has two or three neighbours alive. Fig. 3 shows the numerically calculated probability for a cell to be born or to survive if it has a specific number of neighbours alive, where we have adjusted the field F_- to $F_- = -J(2.8\psi_{\text{alive}} + 5.2\psi_{\text{dead}})$. This gives a slight bias to allow the cell with two alive neighbours to survive and we find that for larger pulse intensity

Conway’s life is obtained (see, e.g., the red marker in Fig. 3). Fig. 4 shows the dynamics under a non-resonant pulsed excitation for different numbers of neighbours, confirming that Conway’s life is attained in the system. In sec. VI we have also shown that Conway’s life can be achieved even in the presence of an additional polarization conserving coupling between neighbours.

Solitons and Patterns

Having established the presence of complex cellular automata, we show examples of the structures that can be formed in the polariton system. Conway’s life is known to support stable self-localized states (Fig. 5(a)) in analogy to the solitons considered in Ref.²⁷ As we operate on a lattice, these can be considered as discrete solitons,⁶⁰ which are also dissipative.³⁵ These solitons are permanent in the system so long as the near-resonant driving field is applied; they do not decay even accounting for the finite polariton lifetime. Another example is shown in Fig.5(bi,bii), which illustrates a rotating soliton. In addition, since bistability at each lattice site exists for some range of detuning (Δ), these solitons and the cellular automaton behaviour in general survives in the presence of disorder (see sec. IV).

Conway’s life also supports propagating oscillating solitons, known as gliders or spaceships (see Fig. 5(ci-cv)), which can be generated in a train using a glider gun (Fig. 5(di,dii)). Collisions between gliders give rise to the formation of a very wide variety of intricate structures, such as exploding patterns (Fig. 5(ei,eii), cf.³³), puffer trains (Fig. 5(fi,fii), cf.³⁴), and the possibility of ordered or chaotic patterns (see sec. II, c.f.³¹). The proof of universal completeness of cellular automata can be established considering signals carried by “ladders” (see sec. I). The sensitivity of our result in Fig. 3 shows that stable lasers with less than 1% intensity fluctuation will be required. We note that intensity fluctuations on the scale of 0.02% are used in polariton experiments.⁶¹

Conclusion

We predict that when a particular stimulus is applied to a polariton lattice, namely a series of identical non-resonant excitation pulses, artificial life can appear in the form of a cellular automaton. This allows the realization of a variety of fundamental nonlinear optical structures under the same conditions, such as solitons, oscillating solitons, breathers, and various patterns. The complexity that arises from the combination of these phenomena is encapsulated within the simple update rules of the automaton. This further shows that polariton solitons are universally complete, even in the presence of dissipation and disorder.

Acknowledgments

This work was supported by the Ministry of Education (Singapore) grant 2017-T2-1-001.

I Other cellular automata

We varied P_+ and P_- for $F_- = -J(3\psi_{\text{alive}} + 5\psi_{\text{dead}})$ and plotted the probability of a cell to be alive or dead depending on their neighbours as shown in Fig. 6. We found different rules like the life without death (B3/S012345678, using standard notation of automata specifying the number of neighbours needed for a cell to be born/survive) and the rule (B3/S0123456) where a cell is born if it has three alive neighbours and survives if it has less than seven alive neighbours. In the case of the Life without death automaton, we take the parameters corresponding to the red spot in Fig. 6 while the green spot indicates the parameters for which we achieve the rule B3/S0123456.

To show that the rule B3/S0123456 is universally complete, we follow Ref.,⁶² which previously showed that the Life without death automaton is universally complete. The proof was based on considering signals in the form of repeating structures, known as “ladders”, that grow from a finite seed (Fig. 7(ai)) in a particular direction as shown in Fig. 7(aii). If ladders

can be terminated, turned, and blocked by other ladders then they can be suitably combined into logic gates ("OR", "AND", "NOT") to realize universal completeness.⁶² These situations are demonstrated in Figs. 7(bi-dii) for the rule B3/S0123456.

It should be noted that when one ladder is used to block another, the relative position of ladders is important. If ladders have the incorrect relative position, then their collision creates extra unnecessary fluctuations in the system, called "lava",⁶² which may divert the propagation of the ladder into a different direction. As the horizontal periodicity of the considered ladders is four and the horizontal ladder can collide with an occupied or unoccupied portion of the vertical ladder, there are a total of eight possible relative shifts denoted by (h, v) , where $h \in \mathbb{Z}_4$ and $v \in \mathbb{Z}_2$ are the horizontal and vertical shifts respectively (note that in Ref.⁶² these shifts are called phase shifts, but we avoid this terminology here so as to not confuse with an optical phase). In Fig. 7(di), two ladders incident from the left have phases $(0,0)$ and $(2,1)$ and are blocked by the ladder on the right. In Fig. 7(ei), the horizontal ladder will collide with the vertical ladder at the unoccupied portion of the vertical ladder, which will not result in the correct blocking behaviour. However, ladders can also be shifted using particular seeds. For example, the situation in Fig. 7(eii), causes the approaching ladder to shift in space so as to collide with the correct relative position with respect to the blocking ladder as shown in Fig. 7(eiii). In this way clean blocking can always be arranged by shifting ladders appropriately between collisions.

II Chaos in cellular automata

So far we have seen that different patterns emerge from Conway's life, including stable, periodic, and moving patterns. Here we provide an example of chaotic behaviour. We start with the initial condition shown in Fig. 8(ai), which gives rise to Fig. 8(aii) after 59 time steps. Changing the initial condition by just one cell to that of Fig. 8(bi), we arrive at a

completely different pattern (see Fig. 8(bii)) after the same number of iterations.

III Materials

Two-dimensional polariton lattices have been intensely developed using GaAs,^{47,48,52,53} so these are currently the most appropriate materials for our proposal. Of course real systems also come with an inevitable disorder, which in principle can destroy polariton solitons. In our system, while the stationary states plotted in Fig. 1(c) can be shifted in the presence of disorder, it is notable that bistability survives over some range of detunings, Δ . Furthermore, introducing a distribution of values of Δ varying from site-to-site we found that cellular automaton rules could persist provided that the strength of disorder is below a finite threshold, estimated around $30 \mu\text{eV}$ (see sec. IV) in GaAs, which is comparable to the disorder of state-of-the-art lattices.⁶³ As our scheme is generic it could also be compatible with materials capable of operation at higher temperatures. For example, Te and Se-based micropillars are in development and could be assembled in the same way as their GaAs predecessors.^{64,65}

IV Effect of disorder

In Fig. 9 we calculated the success rate in the presence of disorder, represented by variation in the detuning Δ at different lattice sites. The disorder in Δ is taken with a uniform distribution with peak-to-peak magnitude $\delta\Delta$. It is notable that when the disorder strength is below some limiting threshold, different automaton rules are obtained with 100% accuracy. Even above the limiting threshold the success rate remains high. It should also be noted that these curves only represent a lower bound on the success rate for a given task. If we consider the on-site disorder of the micropillar of the order of $30 \mu\text{eV}$, then with polariton

lifetime 1.8 ps, the disorder is approximately 0.09 in a dimensionless unit (see the gray vertical line in Fig. 9). Even if some configurations of an automaton do not update with 100% accuracy, the configurations that do update correctly may be sufficient for a particular task, e.g., formation of ladder, creation of a propagating soliton or implementation of an imaging processing algorithm. We have separately verified that in the presence of disorder at the level of 0.09 in our dimensionless units all the structures required for universal computation are perfectly maintained.

V Pulse sequence

As mentioned earlier, one non-resonant pulse of the form $P_{\pm}(t) = P_{\pm}e^{-\Gamma_R t}$ is needed for each automaton update. As an example we show how an oscillating soliton-blinker updates to the next state after applying the pulse. Initially we start with the configuration given by Fig. 10(j) and solve Eq. 1 with F_+ along with $F_- = -J(2.8\psi_{\text{alive}} + 5.2\psi_{\text{dead}})$ for time unit, $t = (0, 20)$. Then we apply the non-resonant pulse to all lattice sites (whose amplitude is indicated by red dot in Fig. 3) as shown by dotted curves in Fig. 10. The steady state updates to Fig. 10(k), which we expect if the system follows Conway's life as depicted in Fig. 5(bi-bii).

VI Effect of same polarization coupling

To check the effect of the same polarization coupling with the neighbours we add a term $J_P \sum_{\langle m \rangle} \psi_{m,\pm}$ with Eq. 1 such that the dynamics of the micropillars are governed by the

following equation

$$i\frac{\partial\psi_{n\pm}}{\partial t} = \left(-\Delta + |\psi_{n\pm}|^2 + \alpha_2|\psi_{n\mp}|^2 + iP_{\pm}(t) - \frac{i}{2}\right)\psi_{n\pm} + J_P \sum_{\langle m \rangle} \psi_{m,\pm} + J \sum_{\langle m \rangle} \psi_{m,\mp} + F_{\pm}. \quad (2)$$

Next we perform all the steps as described earlier. Indeed, the Conways life can be achieved by choosing proper values of the incoherent pulses (see Fig. 11). In the calculation we have chosen $J_P = J = 0.01$, however, we have checked that the Conways life still exists for $J_P > J$ as long as J_P is small ($J_P \ll 1$).

VII Continuous model

In this section we model the system with a continuous wave-function to represent the coupled exciton-polariton micropillars shown in Fig. 12(a). The diameter of the micropillars is chosen to be $5.3 \mu\text{m}$ ⁶⁶ and the separation between the micropillars is $8 \mu\text{m}$ along the vertical and horizontal directions. To realize the diagonal couplings with the same strength as the horizontal and vertical ones we take the diagonal channels wider. Such a structure with channel connecting two pillars was studied in Refs.^{67,68} The width of the channels along the vertical and horizontal direction is taken as $0.5 \mu\text{m}$ and those along the diagonal and anti-diagonal direction is taken as $2 \mu\text{m}$. The depths of the micropillars as well as the channels are taken to be around 4.5 meV . The polariton mass and lifetime are taken as $3 \times 10^{-5}m_e$, where m_e is the free electron mass, and 3 ps , respectively. Due to the shape anisotropy of the channels a splitting between modes polarized parallel and perpendicular to the channel naturally occurs inside them. We take the polarization splitting inside channels as $V_T = V_{avg}/\Delta L$, where V_{avg} is the average splitting in the system which is taken as $0.75 \text{ meV } \mu\text{m}$ and ΔL is the width of the respective channels. Since different channels have different orientations, a phase factor $\exp(2i\phi)$ appears in V_T , where ϕ is the angle of the channels, to

ensure that the polarization splitting is always in the correct direction (this phase factor is readily derived from first writing a splitting between x and y directions and performing a rotation). The phase factors are shown in Fig. 12(b). Due to the symmetry of the unit cell it is clear that there will be no polarization splitting inside the pillars. The spatial profiles of the real and imaginary parts of the polarization splitting is shown in 12(c-d), respectively. Now that all the ingredients are ready, we start by solving the following driven-dissipative Gross-Pitaevskii equation:

$$i\hbar \frac{\partial \psi_{\pm}(\vec{x})}{\partial t} = \left(-\frac{\hbar^2}{2m} \left(\frac{\partial^2}{\partial x^2} + \frac{\partial^2}{\partial y^2} \right) + V(\vec{x}) - \Omega_0 - \frac{i\Gamma}{2} + \alpha_1 |\psi_{\pm}(\vec{x})|^2 + \alpha_2 |\psi_{\mp}(\vec{x})|^2 + iP_{\pm}(t) \right) \psi_{\pm} + V_T(\vec{x}, \phi) \Psi_{\mp} + F_{\pm}. \quad (3)$$

Here $V(\vec{x})$ is the potential profile represented in Fig. 12(a) and Ω_0 is the energy of the resonant pump, which we take 1.1 meV. To find the suitable parameters easily, we move to dimensionless units with the following transformations $t \rightarrow \hbar t/\Gamma$, $\vec{x} \rightarrow \hbar \vec{x}/\sqrt{2m\Gamma}$, $\psi \rightarrow \psi \sqrt{\Gamma/\alpha_1}$

$$i \frac{\partial \psi_{\pm}(\vec{x})}{\partial t} = \left(-\frac{\partial^2}{\partial x^2} - \frac{\partial^2}{\partial y^2} + V(\vec{x}) - \Omega_0 - \frac{i}{2} + |\psi_{\pm}(\vec{x})|^2 + \alpha_2 |\psi_{\mp}(\vec{x})|^2 + iP_{\pm}(t) \right) \psi_{\pm} + V_T(\vec{x}, \phi) \Psi_{\mp} + F_{\pm} \quad (4)$$

where all the energy scales are normalized by Γ , α_2 by α_1 , and $F \rightarrow F \sqrt{\alpha_1/\Gamma^3}$. Initially, we vary the pump very slowly to achieve the hysteresis curve given by Fig. 12(e). The characteristic of the hysteresis curves are the same for all the micropillars. Next we fix F_+ indicated by the vertical gray line of Fig. 12(e), which corresponds to $F_0 = 0.22$. Then we apply the F_- pump of the form $F_- = -\eta(2.8\psi_{\text{alive}} + 5.2\psi_{\text{dead}})$, where $\eta = 0.01$ in the dimensionless form, ψ_{alive} corresponds to the steady state solution of Eq. (4) with all the sites alive, and ψ_{dead} corresponds to the steady state solution with all the sites are dead in presence of $F_+ = F_0$.

The effect of F_- can be seen clearly in Fig. 12(f) where the configuration corresponding to three alive neighbours has the minimum $|\psi_-|^2$. This is equivalent to Fig. 1(d). As discussed earlier this is a very crucial step, which ensures that with the choice of proper parameter of P_{\pm} the states which are initially dead having three alive neighbours become alive, whereas all other initially dead cells with different neighbours remain dead. Next we vary P_+ and P_- simultaneously in presence of F_+ and F_- using the periodic boundary conditions. Indeed, by scanning the space spanned by P_+ and P_- , Conway's life can be obtained, which is indicated by the red dot in Fig. 13. Further in Fig. 14 we have shown that the four configurations lying at the border in Fig. 13 can survive with the 0.02% fluctuation of P_{\pm} .⁶¹

References

- (1) Sanvitto, D. and Kena-Cohen, S., ‘The road towards polaritonic devices’, *Nature Mater.* **15**, 1061 (2016).
- (2) Amo, A. , Pigeon, S. , Sanvitto, D., Sala, V. G., Hivet, R., Carusotto, I., Pisanello, F., Lemenager, G. , Houdre, R., Giacobino, E., Ciuti, C., and Bramati, A., ‘Polariton Superfluids Reveal Quantum Hydrodynamic Solitons’, *Science* **332**, 1167 (2011).
- (3) Grosso, G., Nardin, G., Morier-Genoud, F., Leger, Y., and Deveaud-Pledran, B., ‘Soliton Instabilities and Vortex Street Formation in a Polariton Quantum Fluid’, *Phys. Rev. Lett.* **107**, 245301 (2011).
- (4) Sich, M., Krizhanovskii, D. N., Skolnick, M. S., Gorbach, A. V., Hartley, R., Skryabin, D. V., Cerda-Mendez, E. A., Biermann, K., Hey, R., and Santos, P. V., ‘Observation of bright polariton solitons in a semiconductor microcavity’, *Nat. Photon.* **6**, 50(2012).
- (5) Sich, M., Fras, F., Chana, J. K., Skolnick, M. S., Krizhanovskii, D. N., Gorbach, A. V., Hartley, R., Skryabin, D. V., Gavrillov, S. S., Cerda-Mendez, E. A., Biermann, K., Hey, R., and Santos, P. V., ‘Effects of Spin-Dependent Interactions on Polarization of Bright Polariton Solitons’, *Phys. Rev. Lett.* **112**, 046403 (2014).
- (6) Goblot, V., Nguyen, H. S., Carusotto, I., Galopin, E., Lemaître, A., Sagnes, I., Amo, A., and Bloch, J., ‘Phase-Controlled Bistability of a Dark Soliton Train in a Polariton Fluid’, *Phys. Rev. Lett.* **117**, 217401 (2016).
- (7) Walker, P. M., Tinkler, L., Royall, B., Skryabin, D. V., Farrer, I., Ritchie, D. A., Skolnick, M. S., and Krizhanovskii, D. N., ‘Dark Solitons in High Velocity Waveguide Polariton Fluids.’, *Phys. Rev. Lett.* **119**, 097403 (2017).
- (8) Flayac, H., Solnyshkov, D. D., and Malpuech, G., ‘Oblique half-solitons and their generation in exciton-polariton condensates’, *Phys. Rev. B* **83**, 193305 (2011).

- (9) Pinsker, F. and Flayac, H., ‘On-Demand Dark Soliton Train Manipulation in a Spinor Polariton Condensate’, *Phys. Rev. Lett.* **112**, 140405 (2014).
- (10) Chana, J. K., Sich, M., Fras, F., Gorbach, A. V., Skryabin, D. V., Cancellieri, E., Cerda-Mendez, E. A., Biermann, K., Hey, R., Santos, P. V., Skolnick, M. S., and Krizhanovskii, D. N., ‘Spatial Patterns of Dissipative Polariton Solitons in Semiconductor Microcavities’, *Phys. Rev. Lett.* **115**, 256401 (2015).
- (11) Walker, P. M., Tinkler, L., Skryabin, D. V., Yulin, A., Royall, B., Farrer, I., Ritchie, D. A., Skolnick, M. S. and Krizhanovskii, D. N., ‘Ultra-low-power hybrid light-matter solitons’, *Nature Comm.* **6**, 8317 (2015).
- (12) Cancellieri, E., Chana, J. K., Sich, M., Krizhanovskii, D. N., Skolnick, M. S., and Whittaker, D. M., ‘Logic gates with bright dissipative polariton solitons in Bragg cavity systems’, *Phys. Rev. B* **92**, 174528 (2015).
- (13) Christmann, G., Tosi, G., Berloff, N. G., Tsotsis, P., Eldridge, P. S., Hatzopoulos, Z., Savvidis, P. G. and Baumberg, J. J., ‘Polariton ring condensates and sunflower ripples in an expanding quantum liquid’, *Phys. Rev. B* **85**, 235303 (2012).
- (14) Cristofolini, P., Dreismann, A., Christmann, G., Franchetti, G., Berloff, N. G., Tsotsis, P., Hatzopoulos, Z., Savvidis, P. G., and Baumberg, J. J., ‘Optical Superfluid Phase Transitions and Trapping of Polariton Condensates’, *Phys. Rev. Lett.* **110**, 186403 (2013).
- (15) Saito, H., Aioi, T., and Kadokura, T., ‘Order-Disorder Oscillations in Exciton-Polariton Superfluids’, *Phys. Rev. Lett.* **110**, 26401 (2013).
- (16) Whittaker, C. E., Dzurnak, B., Egorov, O. A., Buonaiuto, G., Walker, P. M., Cancellieri, E., Whittaker, D. M., Clarke, E., Gavrilov, S. S., Skolnick, M. S., and Krizhanovskii, D. N., ‘Polariton Pattern Formation and Photon Statistics of the Associated Emission’, *Phys. Rev. X* **7**, 031033 (2017).

- (17) Diaz-Camacho, G., Tejedor, C., and Marchetti, F. M., ‘Spontaneous patterns in coherently driven polariton microcavities’, *Phys. Rev. B*, **97**, 245309 (2018).
- (18) Keeling, J. and Berloff, N. G., ‘Spontaneous Rotating Vortex Lattices in a Pumped Decaying Condensate’, *Phys. Rev. Lett.* **100**, 250401 (2008).
- (19) Ma, X., Egorov, O. A., and Schumacher, S., ‘Creation and Manipulation of Stable Dark Solitons and Vortices in Microcavity Polariton Condensates’, *Phys. Rev. Lett.* **118**, 157401 (2017).
- (20) Ma, X. and Schumacher, S., ‘Vortex-vortex control in exciton-polariton condensates’, *Phys. Rev. B*, **95**, 235301 (2017).
- (21) Lewandowski, P., Luk, S. M. H., Chan, C. K. P., Leung, P. T., Kwong, N. H., Binder, R., and Schumacher, S., ‘Directional optical switching and transistor functionality using optical parametric oscillation in a spinor polariton fluid’, *Opt. Express*, **25**, 31056 (2017).
- (22) Amo, A. and Bloch, J., ‘Exciton-polaritons in lattices: A non-linear photonic simulator’, *Comptes Rendus Physique* **17**, 934 (2016).
- (23) Flayac, H. and Savenko, I. G., ‘An exciton-polariton mediated all-optical router’, *Appl. Phys. Lett.* **103** 201105 (2013).
- (24) Marsault, F., Nguyen, H. S. , Tanese, D., Lemaitre, A., Galopin, E., Sagnes, I., Amo, A., and Bloch, J., ‘Realization of an all optical exciton-polariton router’, *Appl. Phys. Lett.* **107**, 201115 (2015).
- (25) Tanese, D., Flayac, H., Solnyshkov, D., Amo, A., Lemaitre, A., Galopin, E., Braive, R., Senellart, P., Sagnes, I., Malpuech, G., and Bloch, J., ‘Polariton condensation in solitonic gap states in a one-dimensional periodic potential’, *Nature Comm.* **4**, 1749 (2013).
- (26) Cerda-Mendez, E. A., Sarkar, D., Krizhanovskii, D. N., Gavrilov, S. S., Biermann, K.,

- Skolnick, M. S., and Santos, P. V., ‘Exciton-Polariton Gap Solitons in Two-Dimensional Lattices’, *Phys. Rev. Lett.*, **111**, 146401 (2013).
- (27) Ostrovskaya, E. A., Abdullaev, J., Fraser, M. D., Desyatnikov, A. S., and Kivshar, Y. S., ‘Self-localization of polariton condensates in periodic potentials’, *Phys. Rev. Lett.* **110**, 170407 (2013).
- (28) Ohadi, H., Dreismann, A., Rubo, Y. G., Pinsker, F., del Valle-Inclan Redondo, Y., Tsintzos, S. I., Hatzopoulos, Z., Savvidis, P. G., and Baumberg, J. J., ‘Spontaneous Spin Bifurcations and Ferromagnetic Phase Transitions in a Spinor Exciton-Polariton Condensate’, *Phys. Rev. X* **5**, 031002 (2015).
- (29) Manni, F., Lagoudakis, K. G., Liew, T. C. H., Andre, R., and Deveaud-Pledran, B., ‘Spontaneous Pattern Formation in a Polariton Condensate’, *Phys. Rev. Lett.* **107**, 106401 (2011).
- (30) Christmann, G., Tosi, G., Berloff, N. G., Tsotsis, P., Eldridge, P. S., Hatzopoulos, Z., Savvidis, P. G., and Baumberg, J. J., ‘Oscillatory solitons and time-resolved phase locking of two polariton condensates’, *New J. Phys.* **16**, 103039 (2014).
- (31) Gavrillov, S. S., ‘Polariton Chimeras: Bose-Einstein Condensates with Intrinsic Chaoticity and Spontaneous Long-Range Ordering’, *Phys. Rev. Lett.* **120**, 033901 (2018).
- (32) Flayac, H., Pavlovic, G., Kaliteevski, M. A. and Shelykh, I. A., ‘Electric generation of vortices in polariton superfluids’, *Phys. Rev. B* **85**, 075312 (2012).
- (33) Xue, Y. and Matuszewski, M., ‘Creation and Abrupt Decay of a Quasistationary Dark Soliton in a Polariton Condensate’, *Phys. Rev. Lett.* **112**, 216401 (2014).
- (34) Skryabin, D. V., Kartashov, Y. V., Egorov, O. A., Sich, M., Chana, J. K., Tapia Rodriguez, L. E., Walker, P. M., Clarke, E., Royall, B., Skolnick, M. S., and Krizhanovskii,

- D. N., ‘Backward Cherenkov radiation emitted by polariton solitons in a microcavity wire’, *Nature Comm.* **8**, 1554 (2017).
- (35) Ostrovskaya, E. A., Abdullaev, J., Desyatnikov, A. S., Fraser, M. D., and Kivshar, Y. S., ‘Dissipative solitons and vortices in polariton Bose-Einstein condensates’, *Phys. Rev. A* **86**, 013636 (2012).
- (36) Langton, C. G., ‘Studying artificial life with cellular automata’, *Physica D: Nonlinear Phenomena* **22**, 120 (1986).
- (37) Stephen, W., ‘Statistical mechanics of cellular automata’, *Rev. Mod. Phys.* **55**, 601-644 (1983).
- (38) von Neumann, J., *Theory of Self-reproducing Automata* (edited and completed by A. W. Burks), University of Illinois Press, Urbana and London (1966).
- (39) Wolfram, S., *A New Kind of Science*, Wolfram Media, Inc., Champaign, Illinois (2002).
- .
- (40) Wolfram, S., ed., *Theory and application of cellular automata* (World Scientific, Singapore, 1986).
- (41) Gutowitz, H., ed., *Cellular automata: theory and experiments* (MIT press, Cambridge, 1991).
- (42) Wolfram, S., ‘Universality and complexity in cellular automata’, *Physica D: Nonlinear Phenomena* **10**, 1 (1984).
- (43) Davis, S. L., ‘A Survey of Edge Detection Techniques’, *Computer Graphics and Image Processing*, **12**, 248-270 (1975).
- (44) Chowdhury, R. D., Basu, S., Gupta, S. I., Chaudhuri, P.P., ‘Design of CAECC - cellular automata based error correcting code’, *IEEE Transactions on Computers.* **43** 6 (1994).

- (45) Chang, C., Zhang, Y., Gdong, Y. ‘Cellular Automata for Edge Detection of Images’, IEEE proceedings on Machine Learning and Cybernetics, **26-29** (2004).
- (46) Matthew, C., ‘Universality in Elementary Cellular Automata’; Griffeath, D. and Moore, C. ‘Life Without Death is P-complete’, Complex Systems **10** 437-447 (1996) ; Neary, T., and Woods, D., ‘P-completeness of cellular automaton Rule 110’; Adamatzky, A. (Ed.) (2002) Collision-Based Computing, Springer; Smith, R. A., ‘Simple computation-Universal cellular Spaces’.
- (47) Kim, N. Y., Kusudo, K., Wu, C., Masumoto, N., Loffler, A., Hofling, S., Kumada, N., Worschech, L., Forchel, A., and Yamamoto, Y., ‘Dynamical d-wave condensation of exciton-polaritons in a two-dimensional square-lattice potential’, Nature Phys. **7**, 681 (2011).
- (48) Winkler, K., Fischer, J., Schade, A., Amthor, M., Dall, R., Gebler, J., Emmerling, M., Ostrovskaya, E. A., Kamp, M., Schneider, C., and Hofling, S. ‘A polariton condensate in a photonic crystal potential landscape’, New J. Phys. **17**, 023001 (2015).
- (49) Baas, A., Karr, J. P., Eleuch, H., and Giacobino, E., ‘Optical bistability in semiconductor microcavities’, Phys. Rev. A **69**, 023809 (2004).
- (50) Cerna, R., Leger, Y., Paraiso, T. K., Wouters, M., Morier-Genoud, F., Portella-Oberli, M. T., and Deveaud, B., ‘Ultrafast tristable spin memory of a coherent polariton gas’, Nature Comm. **4**, 2008 (2013).
- (51) Takemura, N., Trebaol, S., Wouters, M., Portella-Oberli, M. T., and Deveaud, B., ‘Heterodyne spectroscopy of polariton spinor interactions’, Phys. Rev. B **90**, 195307 (2014).
- (52) Sala, V. G., Solnyshkov, D. D., Carusotto, I., Jacqumin, T., Lemaître, A., Tercas, H., Nalitov, A., Abbarchi, M., Galopin, E., Sagnes, I., Bloch, J., Malpuech, G., and Amo,

- A., ‘Spin-Orbit Coupling for Photons and Polaritons in Microstructures’, *Phys. Rev. X* **5**, 011034 (2015).
- (53) Whittaker, C. E., Cancellieri, E., Walker, P. M., Gulevich, D. R., Schomerus, H., Vaitiekus, D., Royall, B., Whittaker, D. M., Clarke, E., Iorsh, I. V., Shelykh, I. A., Skolnick, M. S., and Krizhanovskii, D. N., ‘Exciton Polaritons in a Two-Dimensional Lieb Lattice with Spin-Orbit Coupling’, *Phys. Rev. Lett.* **120**, 097401 (2018).
- (54) Vladimirova, M., Cronenberger, S., Scalbert, D., Kavokin, K. V., Miard, A., Lemaitre, A., Bloch, J., Solnyshkov, D., Malpuech, G., and Kavokin, A. V., ‘Polariton-polariton interaction constants in microcavities’, *Phys. Rev. B* **82**, 075301 (2010).
- (55) Gippius, N. A., Shelykh, I. A., Solnyshkov, D. D., Gavrilov, S. S., Rubo, Y. G., Kavokin, A. V., Tikhodeev, S. G., and Malpuech, G., ‘Polarization Multistability of Cavity Polaritons’, *Phys. Rev. Lett.* **98**, 236401 (2007).
- (56) Anton, C., Morina, S., Gao, T., Eldridge, P. S., Liew, T. C. H., Martin, M. D., Hatzopoulos, Z., Savvidis, P. G., Shelykh, I. A., and Vina, L., ‘Optical control of spin textures in quasi-one-dimensional polariton condensates’, *Phys. Rev. B* **91**, 075305 (2015).
- (57) Adrados, C., Liew, T. C. H., Amo, A., Martin, M. D., Sanvitto, D., Anton, C., Giacobino, E., Kavokin, A., Bramati, A., and Vina, L., ‘Motion of Spin Polariton Bullets in Semiconductor Microcavities’, *Phys. Rev. Lett.* **107**, 146402 (2011).;
- (58) Anton, C., Liew, T. C. H., Tosi, G., Martin, M. D., Gao, T., Hatzopoulos, Z., Eldridge, P. S., Savvidis, P. G., and Vina, L., ‘Dynamics of a polariton condensate transistor switch’, *Appl. Phys. Lett.* **101**, 261116 (2012).;
- (59) De Giorgi, M., Ballarini, D., Cancellieri, E., Marchetti, F. M., Szymanska, M. H., Tejedor, C., Cingolani, R., Giacobino, E., Bramati, A., Gigli, G., and Sanvitto, D., ‘Control and Ultrafast Dynamics of a Two-Fluid Polariton Switch’, *Phys. Rev. Lett.* **109**, 266407 (2012).

- (60) Egorov, O. A., and Lederer, F., ‘Spontaneously walking discrete cavity solitons’, *Optics Lett.* **38**, 1010 (2013).
- (61) Abbaspour, H., Sallen, G., Trebaol, S., Morier-Genoud, F., Portella-Oberli, T. M., and Deveaud, B., ‘Effect of a noisy driving field on a bistable polariton system’, *Phys. Rev. B* **92**, 165303 (2015).
- (62) Griffeath, D. and Moore, C., ‘Life Without Death is P-complete’, *Complex Systems* **10**, 437 (1996).
- (63) Baboux, F., Ge, L., Jacquemin, T., Biondi, M., Galopin, E., Lemaître, A., Le Gratiet, L., Sagnes, I., Schmidt, S., Tureci, H. E., Amo, A., and Bloch, J., ‘Bosonic Condensation and Disorder-Induced Localization in a Flat Band’, *Phys. Rev. Lett.* **116**, 066402 (2016).
- (64) Klein, T., Klemmt, S., Durupt, E., Kruse, C., Hommel, D., and Richard, M., ‘Polariton lasing in high-quality selenide-based micropillars in the strong coupling regime.’, *Appl. Phys. Lett.* **107**, 071101 (2015).
- (65) Rousseta, J.-G., Pietka, B., Krol, M., Mirek, R., Lekenta, K., Szczytko, J., Borysiuk, J., Suffczynski, J., Kazimierczuk, T., Goryca, M., Smolenski, T., Kossacki, P., Nawrocki, M., and Pacuski, W., ‘Strong coupling and polariton lasing in Te based microcavities embedding (Cd,Zn)Te quantum wells’, *Appl. Phys. Lett.* **107**, 201109 (2015).
- (66) Boulier, T., Bamba, M., Amo, A., Adrados, C., Lemaître, A., Galopin, E., Sagnes, I., Bloch, J., Ciuti, C., Giacobino, E., and Bramati, A., ‘Polariton-generated intensity squeezing in semiconductor micropillars’, *Nat. Commun.* volume **5** 3260 (2014).
- (67) Bayer, M., Gutbrod, T., Reithmaier, J. P., Forchel, A., Reinecke, T. L., Knipp, P. A., Dremin, A. A., and Kulakovskii, V. D., ‘Optical Modes in Photonic Molecules’, *Phys. Rev. Lett.* **81**, 2582 (1998).

- (68) R. Su, S. Ghosh, J. Wang, S. Liu, C. Diederichs, T. C. H. Liew, and Q. Xiong, "Observation of exciton polariton condensation in a perovskite lattice at room temperature", *Nat. Phys.* **16**, 301 (2020).

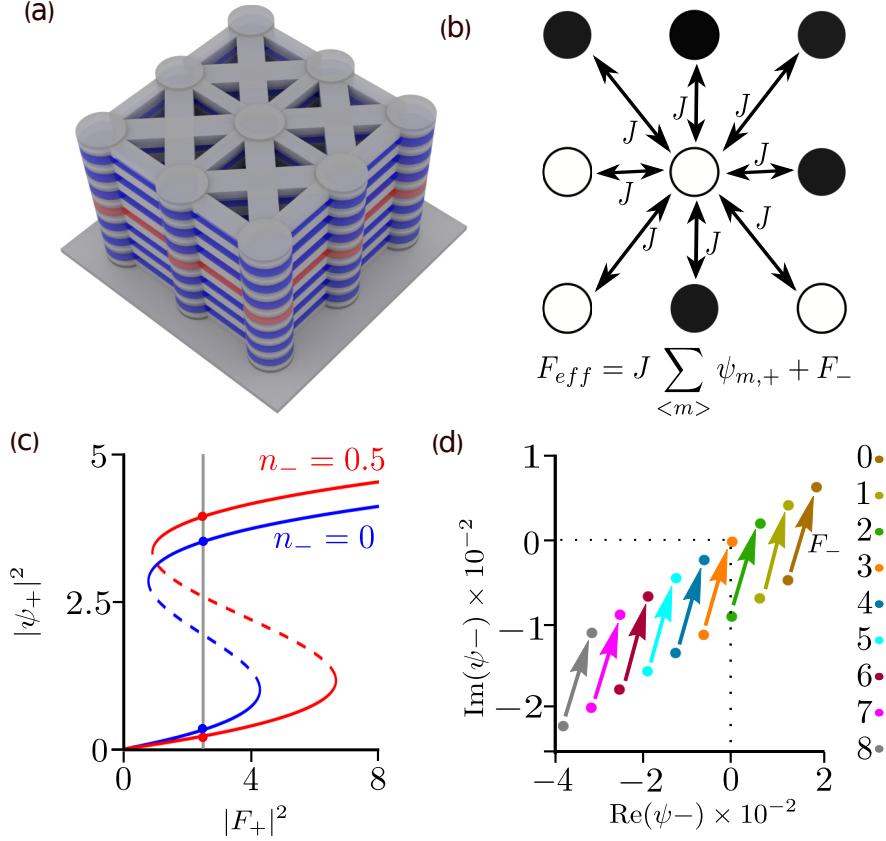


Figure 1: **(a)** A square lattice of coupled cells formed by polariton resonators. Blue and grey denote alternating layers of refractive index, which trap polaritons in the cavity layer (red). The sample is etched in a way to leave channels that connect the resonators. **(b)** Each cell interacts with eight neighbours, which provide an effective driving, F_{eff} . This field depends on how many neighbours are alive and on the constant field F_- . **(c)** Single cell stationary solutions under the condition $J = 0, P_{\pm}(t) = 0$, and $F_- = 0$ with and without the influence of ψ_- . A non-zero population of σ_- particles raises the threshold intensity for reaching the higher ψ_+ state. Parameters: $\Delta = 3, \alpha_2 = -1$.⁵⁴ The grey line shows the fixed continuous driving for which there are two stable solutions (dashed curves correspond to unstable states). **(d)** Neighbour dependent values of the ψ_- field caused by the effective driving, F_{eff} , with (upper points) and without (lower points) the driving field F_- under the condition $P_{\pm}(t) = 0$ for a cell initially in the lower intensity (dead) ψ_+ state. Colours represent different numbers of neighbours in the higher intensity (alive) ψ_+ state. Parameters: $J = 0.01, \alpha_2 = -1$.⁵⁴

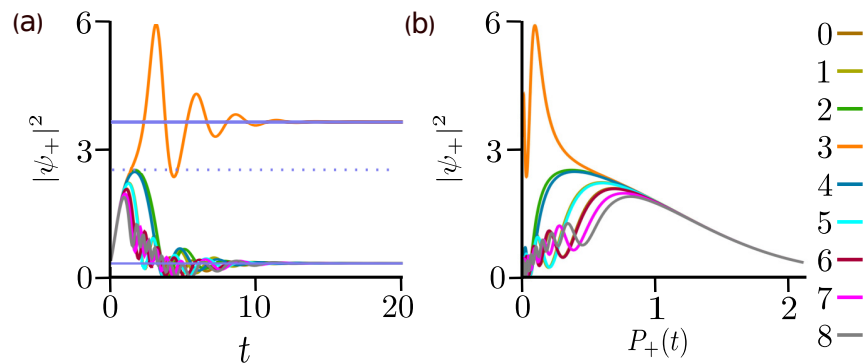


Figure 2: **(a)** Time evolution of ψ_+ after the application of a non-resonant pulse. The solid lines (violet color) represent the stable states. The dotted line represents the unstable state. The figure shows a switching to the higher intensity state if a dead cell has three neighbours alive, while otherwise it remains in the lower intensity state. **(b)** Plot of the σ_+ intensity vs the decaying non-resonant pulse intensity for different numbers of alive neighbours. Parameters: $\Gamma_R = 1$.

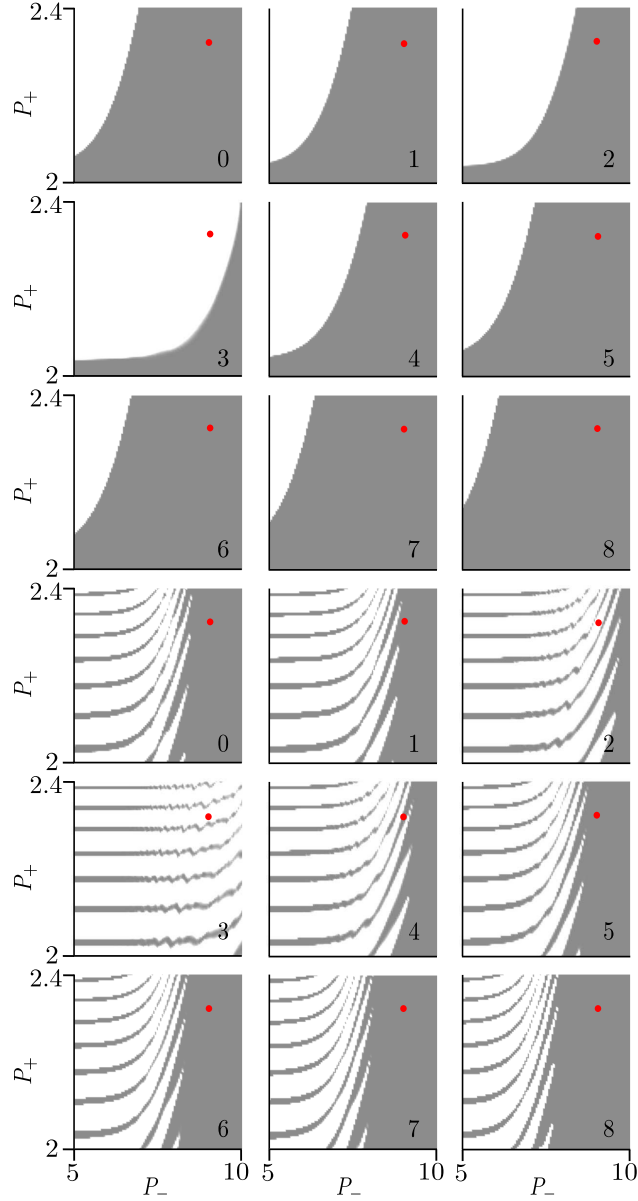


Figure 3: Variation of automaton rules with P_+ and P_- . Each plot shows whether a cell that is initially dead (upper nine plots) or initially alive (lower nine plots) finishes in an alive state after the application of a pulse for different numbers of neighbouring (initially) alive cells (given by the labels in the bottom-right corners of each plot). White corresponds to parameters for which a cell finishes in the alive state, while grey corresponds to parameters for which a cell finishes in the dead state. The red spot indicates a parameter choice for which Conway's life appears. Parameters: $F_- = -J(2.8\psi_{\text{alive}} + 5.2\psi_{\text{dead}})$, $\Delta = 3$, $J = 0.01$, and $\alpha_2 = -1$.

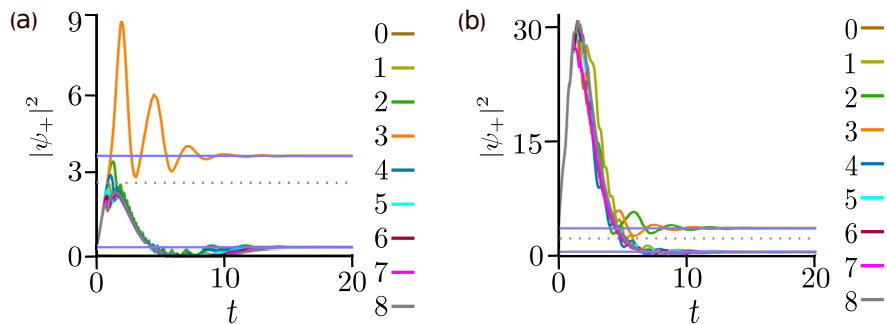


Figure 4: Dynamics of $|\psi_+|^2$ under pulsed excitation for a cell initially dead **(a)** or alive **(b)**. The different coloured curves correspond to different numbers of neighbours (initially) alive. Only configurations where a dead cell has three alive neighbours, or where a cell was initially alive and has two or three alive neighbours results in the cell being alive at the end of the pulse. The amplitude of the pulses were chosen according to the red spot in Fig. 3. Parameters: $F_- = -J(2.8\psi_{\text{alive}} + 5.2\psi_{\text{dead}})$, $\Delta = 3$, $J = 0.01$, and $\alpha_2 = -1$.

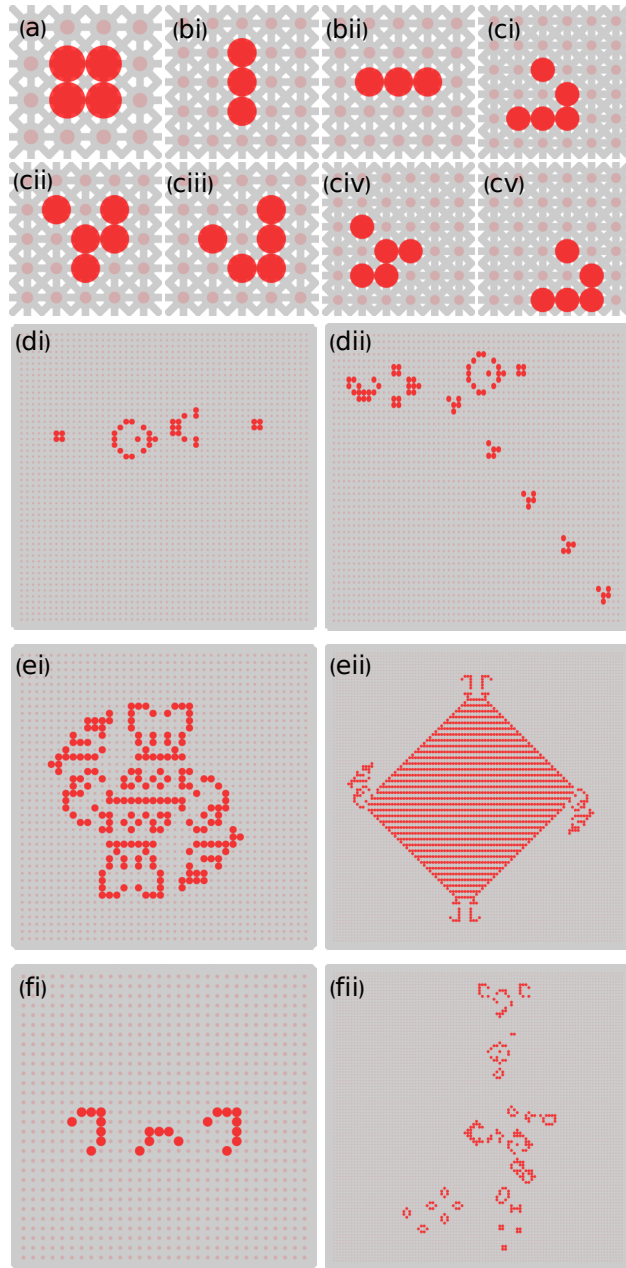


Figure 5: Examples of configurations attained within Conway's life. **(a)** A 2×2 block maintains its form over time. **(bi-bii)** An oscillating soliton (blinker), with periodicity two. **(ci-cv)** A glider, that is, a soliton that translates diagonally in four timesteps. **(di,dii)** A glider gun, that is, starting with the configuration in **(di)**, a train of solitons is emitted as shown in **(dii)**. **(ei,eii)** A soliton explosion where an initial condition **(ei)** fills the whole space over time **(eii)**. **(fi,fii)** An emitting soliton where the initial condition in **(fi)** moves upwards, while also leaving behind a dynamic pattern.

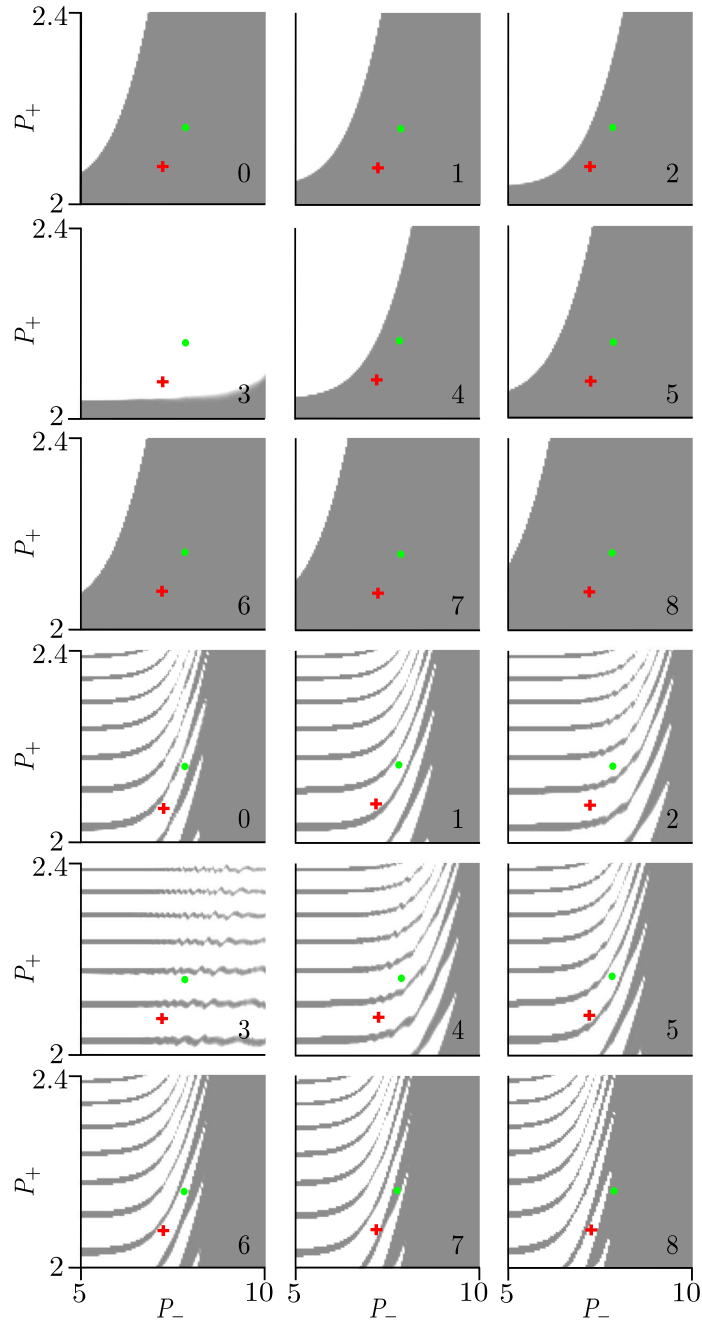


Figure 6: **(a)** Probability for a cell to be in the alive state depending on the number of alive neighbours (marked in the bottom right corner of the plots) for $F_- = -J(3\psi_{\text{alive}} + 5\psi_{\text{dead}})$, for cases when it was initially dead (upper nine plots) and alive (lower nine plots). For the parameters in the white region, the cell finishes in the alive state and for the grey region, it finishes in the dead state. The green dot marks a set of parameters for which the rule B3/S0123456 is obtained, while the red + marks a set of parameters for which Life without death (B3/S012345678) was obtained.

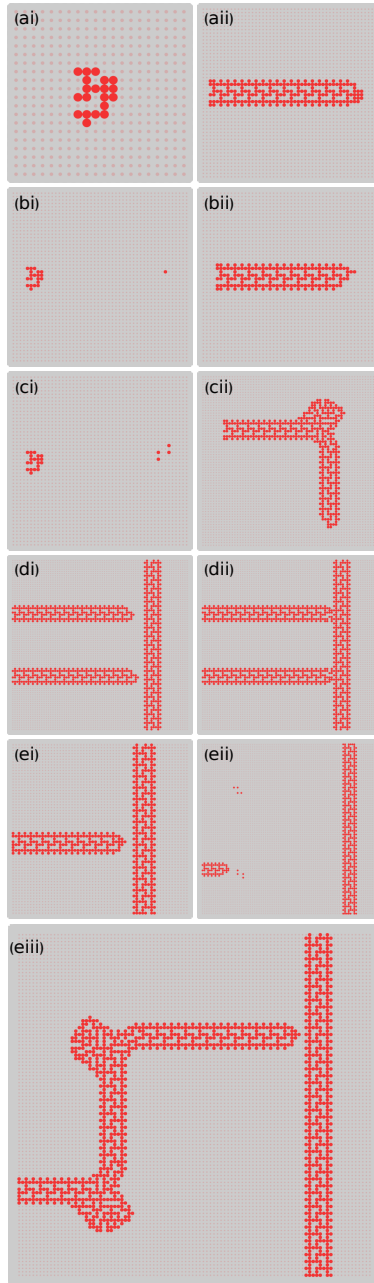


Figure 7: Behaviour of ladders emerging from the rule (B3/S0123456). **(ai)** It is a finite seed that gives a periodic structure that moves in one direction, called a ladder shown in **(aii)**. **(bi,bii)** The propagation of a ladder is ended by a single cell. **(ci,cii)** In the presence of a finite seed a ladder is turned so as to propagate in the perpendicular direction. **(di,dii)** Ladder can be blocked by other ladders. Here two ladders are incident from the left with relative phases $(0,0)$ and $(2,1)$. **(ei-eiii)** The relative displacement of ladders can be shifted, which helps to ensure clean blocking.

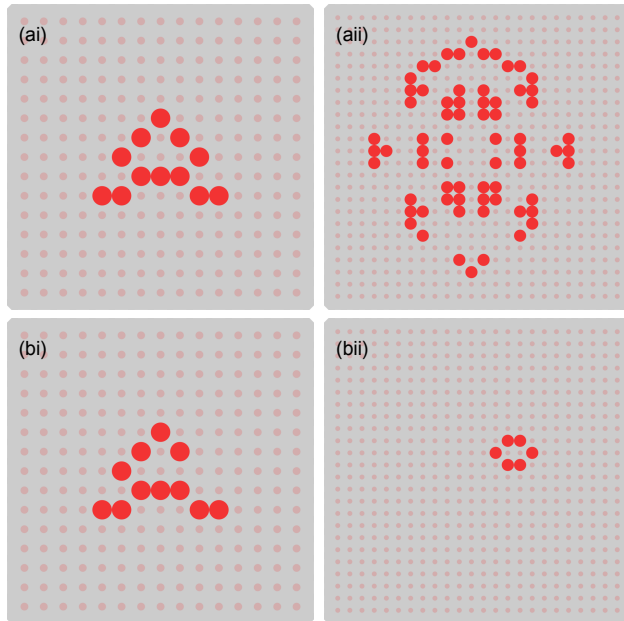


Figure 8: Example of chaotic behaviour in Conway's life. **(ai,aii)** The initial state **(ai)** evolves into the pattern **(aii)** after 59 iterations. **(bi,bii)** The initial state **(bi)** differs from that of **(ai)** by only one cell, and gives rise to a completely different pattern **(bii)** after the same number of iterations.

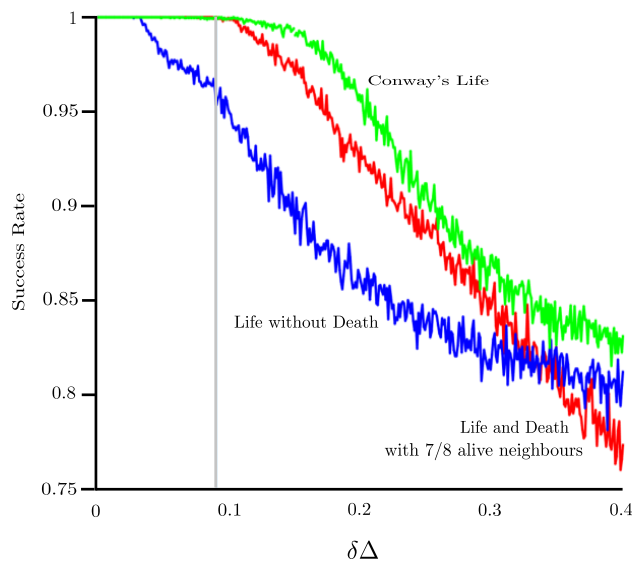


Figure 9: Dependence of the success rate on disorder for different cellular automaton rules. Δ is chosen differently for different lattice sites, using a uniformly distributed random variable with peak-to-peak amplitude $\delta\Delta$. When disorder is below some threshold, cellular automata are still obtained perfectly with 100% success rate. Above this disorder threshold, the success rate slowly decreases.

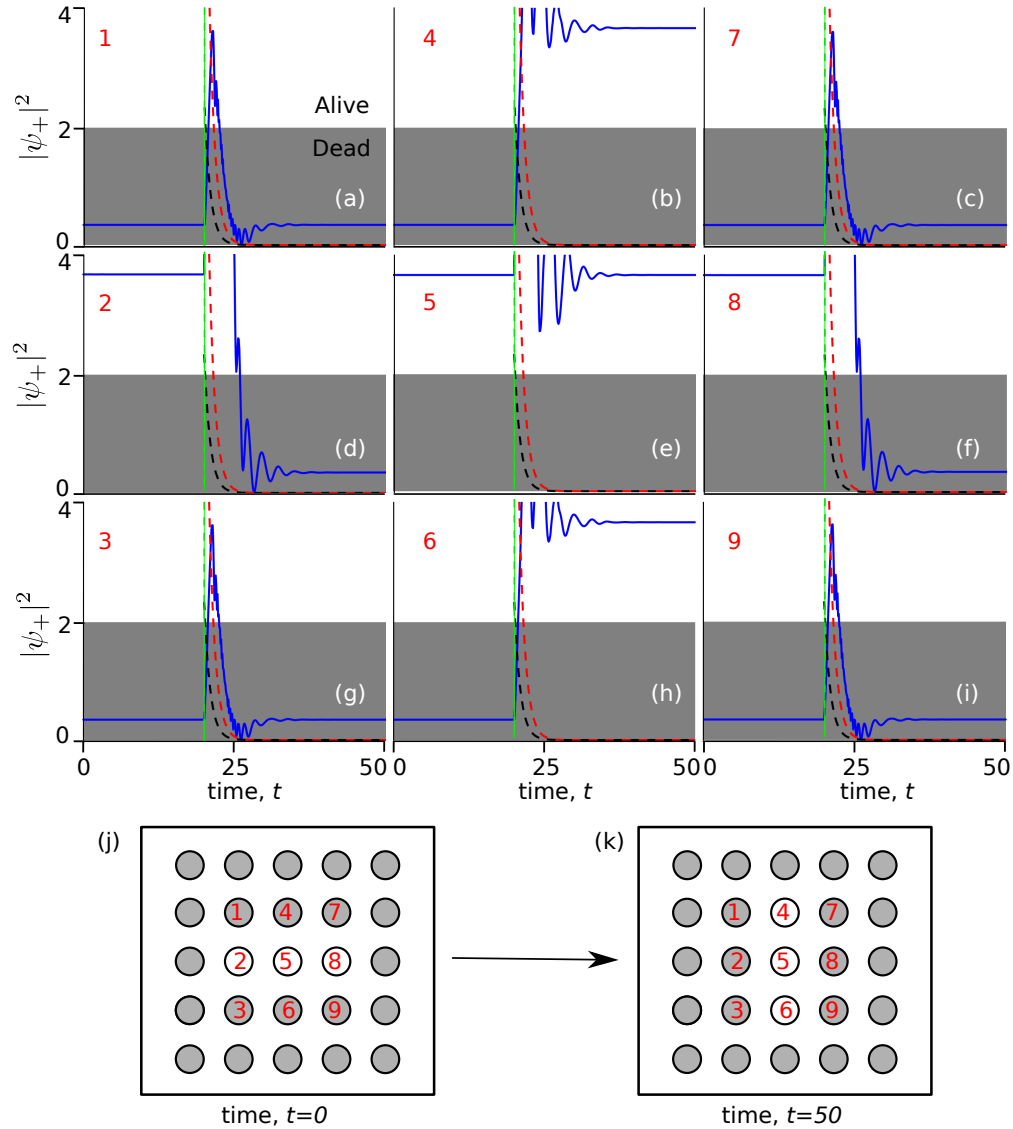


Figure 10: Time evolution of oscillating soliton - blinker which emerges from Conway's life. After applying the pulse the initial state (j) updates to final state (k). The grey region corresponds to a dead state while white to an alive state. Here we plotted the time dynamics only for the centered 3×3 lattice sites indicated by indices 1, 2, 3, ..., 9 (top-left). It shows that initially we start with an alive state in cells (2, 5, 8) and after the pulse two new cells are born (4 and 6) and 5 remains alive. The pulses are indicated by the dotted curves where black represents $P_+(t)$ and red represents $P_-(t)$. The green dotted vertical lines represent the time at which the pulses are injected. The amplitude of the pulses is taken from the red dot in Fig. 3.

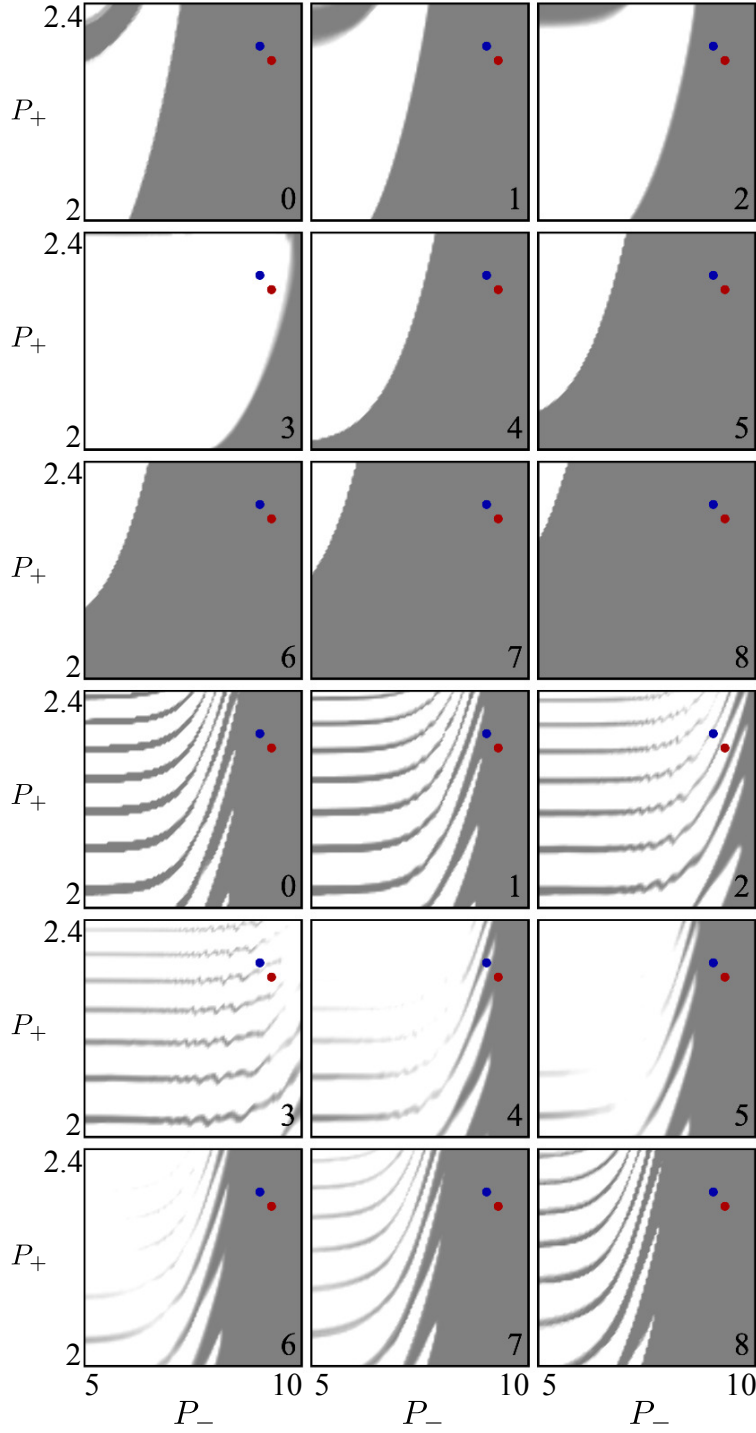


Figure 11: Variation of automaton rules with P_+ and P_- in the tight binding model according to Eq. (2) where polarization conserving coupling with neighbours are also considered. The parameter indicated by the red dot corresponds to the Conways life. The blue dot corresponds to the parameter corresponding to the Conways life shown in Fig 3 where $J_P = 0$. Parameters: $J_P = J = 0.01$, $F_- = -J(2.8\psi_{\text{alive}} + 5.2\psi_{\text{dead}})$ and all other parameters are kept the same as those in Fig. 3.

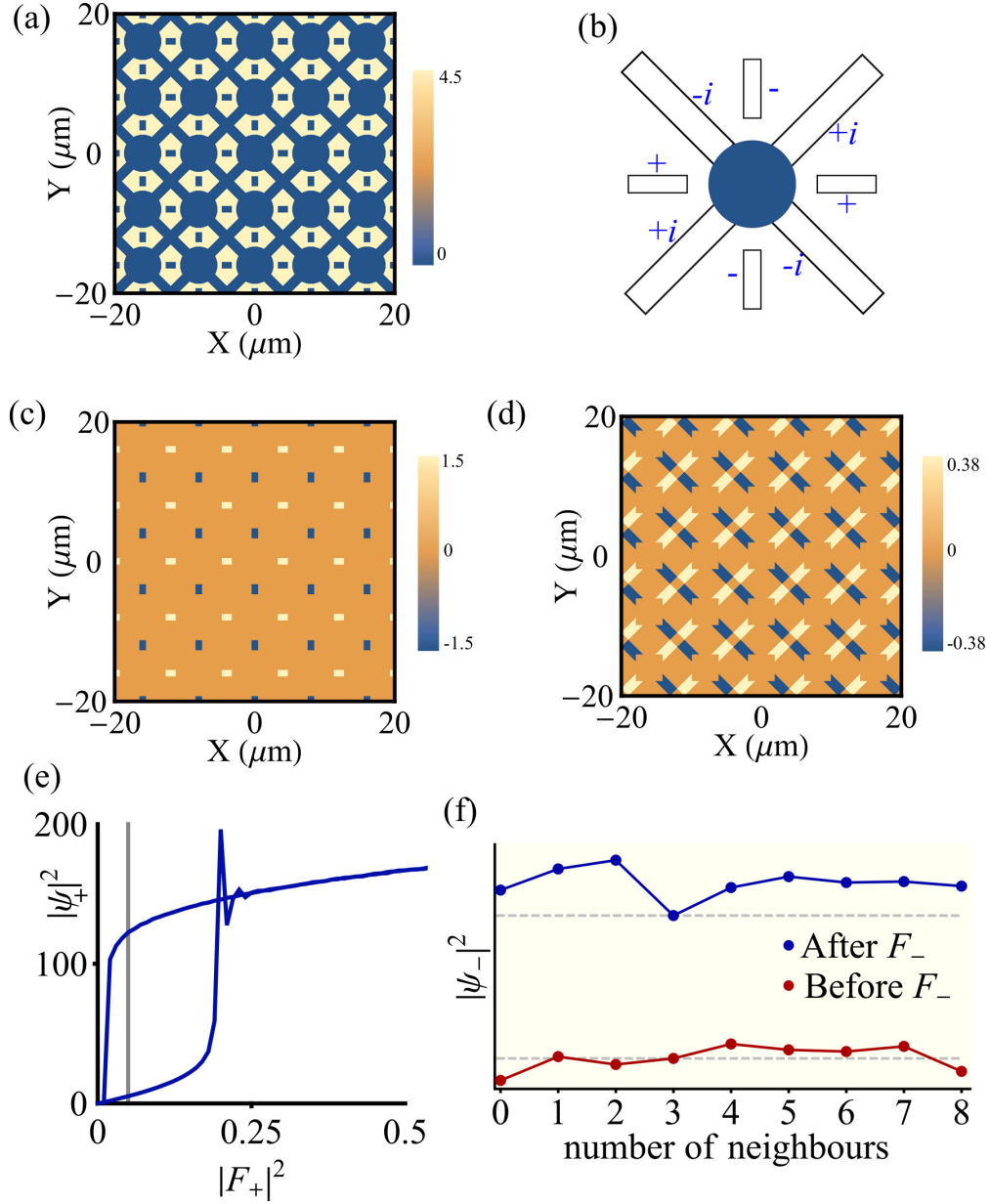


Figure 12: (a) An example of the potential profile of a 5×5 lattice. Each micropillar is connected to its eight neighbours through the channels. (b) Due to their orientations the horizontal and vertical channels have opposite polarization splittings. The polarization splitting inside the diagonal channels have only imaginary parts due to their $\pi/4$ orientation with respect to the x axis and those inside the antidiagonal channels are opposite to the diagonal ones. (c-d) The real and imaginary parts of the polarization splitting, respectively. (e) The bistability curve of the micropillars where the gray horizontal line indicates the $|F_+|^2$ value used in the calculation. (f) The effect of F_- on the initially dead configurations with different number of alive neighbours. After applying F_- the configuration corresponding to three alive neighbours has the minimum $|\psi_-|^2$, similar to Fig. 1(d).

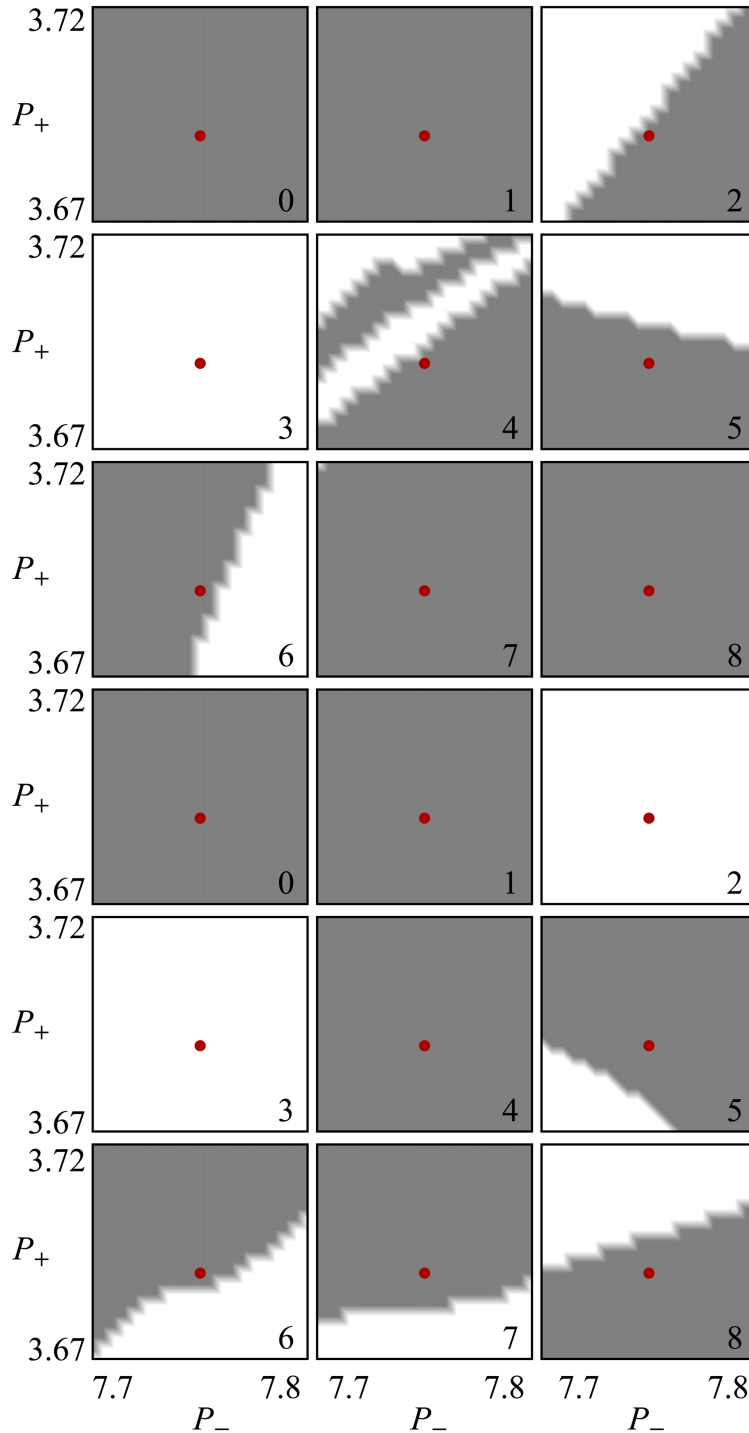


Figure 13: Variation of automaton rules with P_+ and P_- in the continuous model under the periodic boundary condition is depicted here. White corresponds to parameters for which a cell finishes in an alive state, while grey corresponds to parameters for which a cell finishes in a dead state. Corresponding to the nine upper plots, the states were initially dead and alive for the lower nine plots. The red dot indicates a parameter choice for which Conway's life appears. Parameter: $\alpha_2 = -1$.

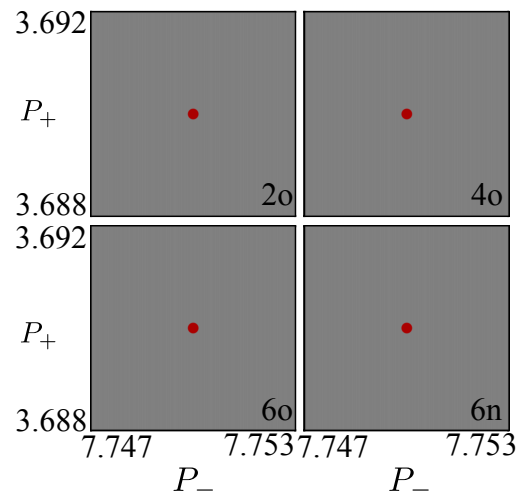


Figure 14: Zoomed view of the 2o, 4o, 6o and 6n configurations, respectively, from the previous figure which show that the chosen parameter can tolerate the 0.02% variation of the incoherent pulses. Here ‘o’ and ‘n’ indicate initially dead and alive states, respectively.